A New Continuous-Time Model for Current-Mode Control with Constant Frequency, Constant On-Time, and Constant Off-Time, in CCM and DCM

Raymond B. Ridley

Virginia Power Electronics Center
Bradley Department of Electrical Engineering
Virginia Polytechnic Institute and State University
Blacksburg, Virginia 24061

Abstract

A new small-signal model for current-mode control of PWM converters is extended for constant on-time control, constant off-time control, and discontinuous conduction mode. Constant on- or off-time converters in CCM have two complex right-half-plane zeros in the current loop feedback, but reduced modulator gain eliminates current-loop instability. The modulator gain exhibits frequency-dependent phase which introduces an extra gain term in the circuit model. The new model for DCM operation does not have RHP zeros in the current feedback loop, but the buck converter exhibits an instability for higher conversion ratios.

I. Introduction

A new small-signal model has been developed for current-mode control [1] which overcomes inaccuracies of previous average models [2-5] and is simpler to use than sampled-data models [6]. This new model provides accurate predictions for frequencies up to half the switching frequency, and correctly shows the current-loop instability which occurs with constant-frequency control.

In this paper, the modeling is extended to cover constant on-time and constant off-time control of converters in the continuous-conduction mode (CCM). Sampled-data analysis is needed to develop the model, but the same approximation can be used as for constant-frequency [1] to obtain a simple model for design.

A new model is also developed for current-mode-controlled converters operating in the discontinuous-conduction mode (DCM). It is shown that this mode of operation does not require any sampled-data modeling, and simple feedforward terms in the model are sufficient to completely describe the system.

II. Review of Constant-Frequency Model

The new current-mode control models are dependent on the use of PWM switch modeling techniques [7], where the nonlinear action of the active and passive switches of the PWM converters are replaced with a simple linear small-signal circuit. Fig. 1 gives the resulting circuit for continuous-conduction mode, and shows how it is connected in the buck, boost, and flyback circuits. The controlled sources of Fig. 1a are determined by the steady-state terminal quantities of the circuit in which the PWM switch is placed.

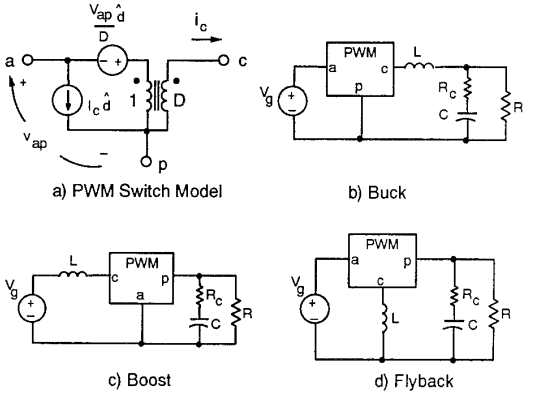

Fig. 1: PWM Switch Model in Power Converters for Continuous-Conduction Mode. *The PWM switch model is invariant for any PWM converter, its gains determined by its steady-state terminal quantities. It is inserted in the power stage circuit, in place of the active switch and passive diode, to provide the power stage small-signal model.*

Fig. 2 shows a buck PWM converter with a current-mode controller. The ramp of the filter inductor current is added to an external sawtooth ramp of slope S_e, and compared to the control voltage to provide the duty cycle signal, d. In [1] it was shown that the current-mode control system requires sampled-data analysis to fully model the dynamics of the current feedback. However, a second-order approximation to a sampled-data transfer function produces a simple new model, the block diagram of which is shown in Fig. 3. The feedback gain blocks for this block diagram are given in Table 1. The power stage model used in Fig. 3 is the same as that shown in Fig. 1 for the appropriate power stage.

An important consequence of the new model is a pair of complex zeros in the current feedback loop, modeled by the gain block $H_e(s)$. The loop closed by feedback of the inductor current can become unstable if it has sufficient gain. With no external ramp, this current loop becomes unstable at a duty cycle of 0.5 when using constant-frequency control. This is the well-known subharmonic oscillation problem.

It is often inconvenient to break the feedback loop with the current information since digital waveforms must usually be modulated with specialized circuitry. Designers characterize their current-mode systems by measuring the control-to-output gain, $\hat{v}_o/\hat{v}_c$, with the current loop closed. The current-loop instability is manifested in this transfer function by a pair of complex poles at half the switching frequency, in addition

CH2873-8/90/0000-0382 $1.00

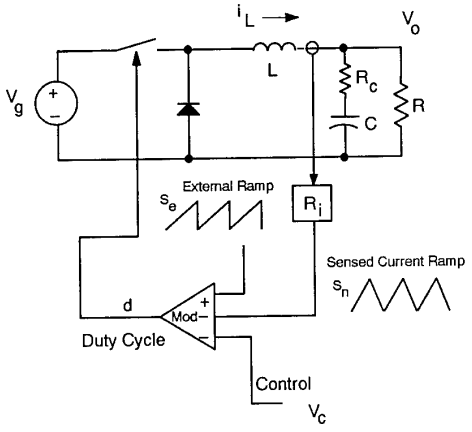

Fig. 2: Current-Mode Control for a Buck Converter. *The inductor current i_L is sensed and scaled by a network with gain R_i. The sensed current ramp is augmented with an external ramp S_e (if necessary) and compared with an error signal v_c to produce the duty cycle control.*

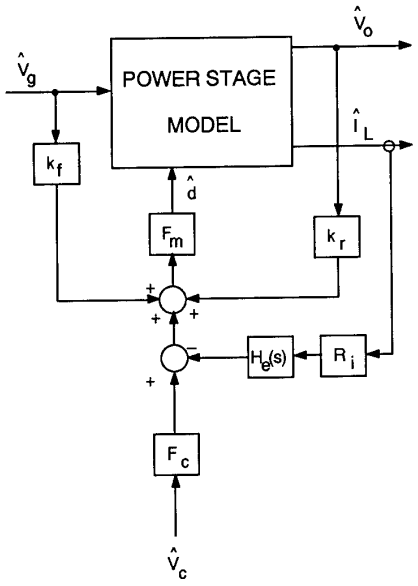

Fig. 3: Small-Signal Block Diagram for Current-Mode Control (CCM). *The accuracy of sampled-data modeling is incorporated in the model by the gain block $H_e(s)$. Feedforward gains k_f and k_r are created when the current feedback loop is closed. The modulator gain block F_c is unity for constant-frequency control, and is frequency dependent for other modulation schemes.*

TABLE 1
Summary of Gain Parameters for Constant-Frequency

	Buck	Boost	Buck-Boost
k_f	$-DK_i\left[1-\frac{D}{2}\right]$	$-\frac{K_i}{2}$	$-DK_i\left[1-\frac{D}{2}\right]$
k_r	$\frac{K_i}{2}$	$\frac{D'^2K_i}{2}$	$\frac{D'^2K_i}{2}$
F_m	$\frac{1}{(S_n+S_e)T_s}$		
F_c	1		
$H_e(s)$	$1+\frac{s}{\omega_n Q_z}+\frac{s^2}{\omega_n^2}$ $\quad Q_z=\frac{-2}{\pi}$		

$$K_i=\frac{R_iT_s}{L}$$

to the dominant low frequency pole expected with current-mode control. Without an external ramp, the Q of this complex pole pair becomes very large as a duty cycle of 0.5 is approached, clearly showing the onset of subharmonic oscillation. The Q of the complex poles is given by

$$Q=\frac{1}{\pi(m_cD'-0.5)} \tag{1}$$

where

$$m_c=1+\frac{S_e}{S_n} \tag{2}$$

An external ramp is used to decrease the Q of the complex pole pair, and stabilize the system.

III. Constant On-Time and Constant Off-Time Control

Constant on-time or constant off-time modulators are sometimes used instead of constant frequency modulators. These control schemes can offer advantages of low audio susceptibility, ease of implementation, or lower power stage weight. The most commonly used scheme is the constant off-time modulator, especially for current-mode control where the inductor current can easily be sensed when the power switch is on.

There are many different schemes which can be used to provide constant on- or off-time modulation. Fig. 4 shows the most common scheme for generating constant off-time control. A PWM ramp signal is started when the power switch is turned on, and this provides the turn-off command when the ramp intersects the modulated control signal, v_c. This scheme gives an on-time pulse of varying width. The falling edge of the PWM output pulse triggers a monostable multivibrator which provides the fixed off-time signal. The falling edge of the monostable output triggers the turn-on of the power switch. Notice that an external ramp is rarely used for constant off-time modulation, and the effect of an external ramp is not considered here.

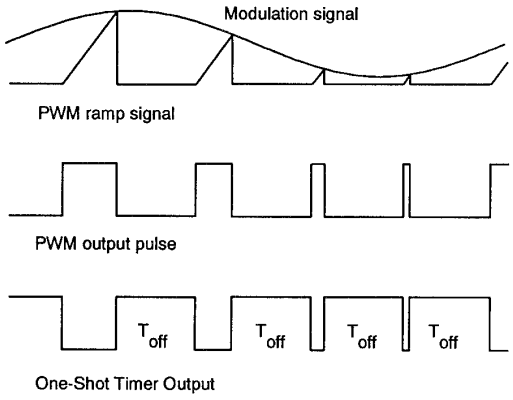

Fig. 4: Constant Off-Time Modulator Waveforms. *A timer is started when the switch is turned off to provide a constant off-time pulse. A ramp is initiated when the switch is turn on, and the intersection of the ramp with the modulation signal is used to provide the signal to turn the switch off. This control scheme has a transfer function with a phase lead.*

It is easy to show that the gain of the constant off-time modulator is given by

$$F_m = \frac{D'}{S_n T_s} \tag{3}$$

Notice that this is the same gain as that for the constant-frequency modulator, multiplied by D'.

In [1], the constant-frequency converter was analyzed using sampled-data techniques just for the current feedback block. The input voltage and output voltage of the converter were held constant for this analysis. Similar analysis can be performed for the constant on- and off-time converters. It can be shown that the natural response of the current feedback block is the same as that for a constant-frequency control which has an external ramp equal to the downslope of the inductor current. The gain of the constant-frequency modulator for this case is the same as that of Eq. (3). The portion of the current-mode model represented by the power stage, current feedback gain, R_i, sampling gain, $H_e(s)$, and modulator gain, F_m, remains the same for the constant on- and off-time control systems.

This portion of the model can be experimentally verified by measuring the current-loop gain of the system. From the model of Fig. 3, the current loop gain is given by

$$T_i(s) = F_m \frac{\hat{i}_L(s)}{\hat{d}(s)} R_i H_e(s) = \frac{L}{RT_s} \frac{1 + sCR}{1 + \frac{s}{\omega_o Q_p} + \frac{s^2}{\omega_o^2}} H_e(s) \tag{4}$$

where

$$\omega_o = \frac{1}{\sqrt{LC}} \tag{5}$$

and

$$Q_p = \frac{1}{\omega_o \left[\frac{L}{R} + CR_c \right]} \tag{6}$$

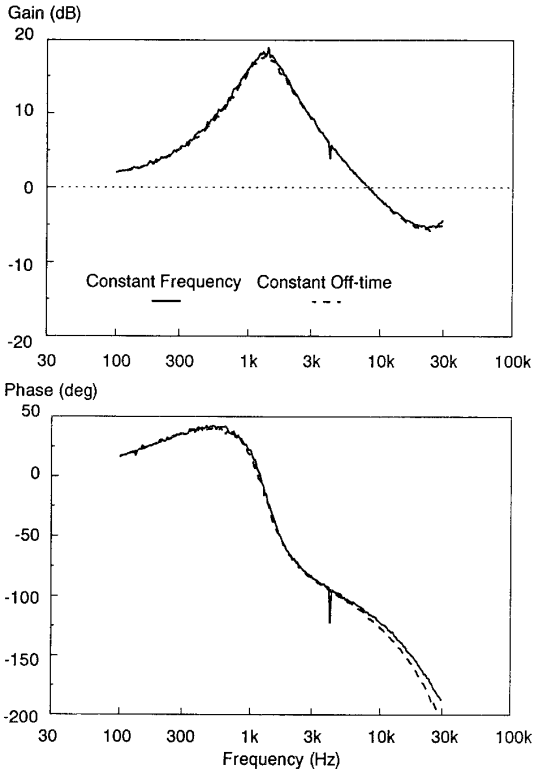

Fig. 5: Current Loop-Gain Measurement for Constant Frequency and Constant Off-Time. *The current loop gain for constant-frequency control with an external ramp equal to the off-slope of the current signal is identical to the current loop gain of the constant off-time system. This loop gain remains invariant with duty cycle for the constant off-time control, remaining stable under all conditions. For constant frequency, the loop gain increases with duty cycle, and can become unstable if insufficient external ramp is used.*

This current loop gain is invariant for all values of line and duty cycle, and the high-frequency portion after the resonant frequency is also invariant for all values of load. The current loop gain for the constant-frequency converter is given by

$$T_i'(s) = \frac{T_i(s)}{D' m_c} \tag{7}$$

For an external ramp of $S_e = S_f$, $m_c = 1/D'$, and the constant frequency and constant off-time current loop gains should be the same. Fig. 5 shows a plot of the current loop gain of these two different systems, measured with digital modulation techniques [8] at the output of the modulator. It can be seen that the two plots are identical up to half the switching frequency, thus confirming the current feedback part of the model in Fig. 3.

The constant form of the current loop gain of Eq. (4) means that subharmonic instability does not occur when using constant on- or off-time control, as is well known. The only way to increase the gain of the current loop is to add a negative external ramp to the system, which is unlikely to be done.

The varying gain of the constant-frequency current-loop gain produces a pair of complex poles at half the switching fre-

quency in the control-to-output transfer function, with a quality factor given by Eq. (1). The fixed current loop gain of the constant on and off-time control schemes produce a control-to-output transfer function which also has a double pole at half the switching frequency, but with a fixed quality factor given by

$$Q = \frac{2}{\pi} \tag{8}$$

The constant off-time modulator described earlier shows an interesting characteristic. Unlike the naturally-sampled constant frequency modulator which has flat gain and phase [9], the constant off-time modulator exhibits a phase-lead characteristic which increases linearly with duty cycle and with frequency. Fig. 6 shows the measured phase characteristics of the constant off-time modulator for different duty cycles, and compares this with the constant-frequency modulator with a duty cycle of 0.45.

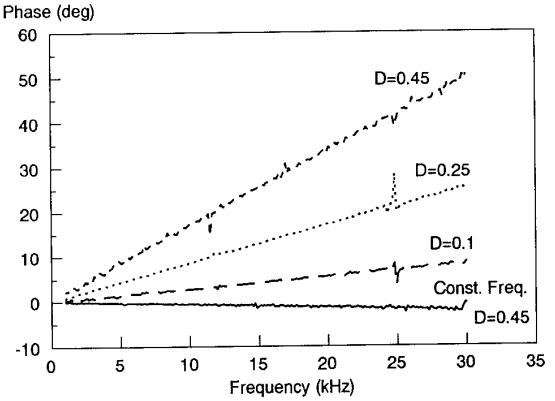

Fig. 6: Constant Off-Time Modulator Phase Measurement. *The constant off-time modulator generated by the scheme shown in Fig. 4 shows a linear phase lead, the slope of which depends on the duty cycle. The constant on-time modulator also shows a phase lead, the slope of which depends upon the complement of the duty cycle, $D' = 1 - D$.*

The modulator with a duty cycle of only 0.1 gives a small phase lead of only 10 degrees at half the switching frequency. However, this phase lead increases to 45 degrees at a duty cycle of 0.5, and to 90 degrees at a duty cycle of 1. The gain of the modulator, not shown in Fig. 6, also shows an increase at higher duty cycles, but this effect is not modeled.

The phase lead of the modulator is modeled in Fig. 3 by the gain F_c , and this is given by

$$F_c = e^{sDT_s/4} \tag{9}$$

for constant off-time, and by

$$F_c = e^{sD'T_s/4} \tag{10}$$

for constant on-time control.

For low duty cycles, the modulator gain of the constant off-time control is close to that of constant frequency control, and the Q of the control-to-output transfer function of the constant-frequency control approaches $2/\pi$. Fig. 7 shows the control-to-output transfer function of a constant frequency and constant off-time buck converter with a duty cycle of 0.1. It can be seen that the gain characteristics are almost exactly the same. The phase characteristics agree well up to higher

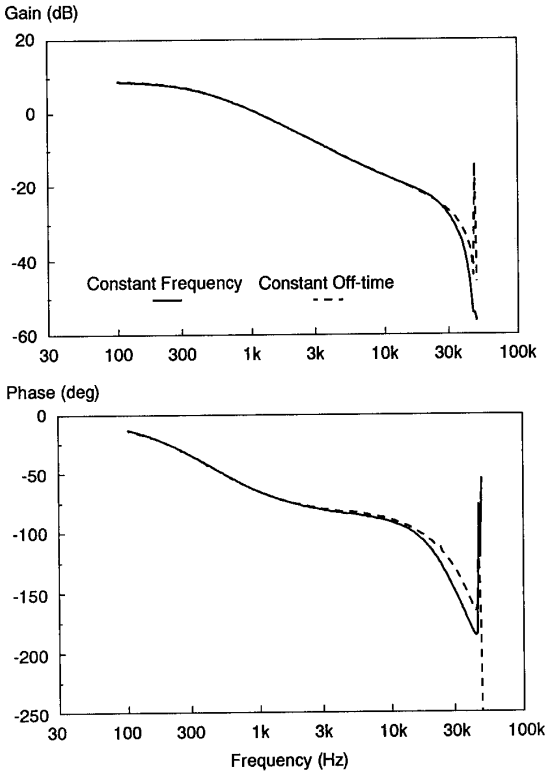

Fig. 7: Control-to-Output Measurement for Constant Frequency and Constant Off-Time. *For very low duty cycles, these transfer functions are almost identical. The phase lead introduced by the modulator is small at low duty cycles, less than 10° at half the switching frequency. Like the constant frequency control system, this transfer function has a pair of poles at half the switching frequency. These poles have a fixed Q of $2/\pi$, regardless of duty cycle.*

frequencies where the small phase lead of the modulator accounts for the differences.

Derivation of feedforward gains k_f and k_r completes the constant on- and off-time models for current-mode control. These gains are derived from the steady-state operating conditions in a similar manner to the gains for constant frequency control. They are needed to complete the model to account for the fact that the current-mode control schemes regulate the peak of the current, not the average of the current. Table 2 summarizes all of the gains for the constant off-time model, and Table 3 summarizes the gains obtained for constant on-time.

Fig. 8 shows the result of the predictions of the model with the gains of Table 2, compared with measured results for a duty cycle of $D = 0.1$. The correlation between measured and theoretical results is excellent up to half the switching frequency.

Fig. 9 shows measurements and predictions for a duty cycle of $D = 0.4$. The agreements between measurements and predictions are again very good up to half the switching frequency. For this larger duty cycle, the phase-lead contribution of the modulator is significant, and it can be seen that the phase at half the switching frequency is much higher than the corresponding phase for the lower duty cycle in Fig. 8.

TABLE 2

Summary of Gain Parameters for Constant Off-Time

	Buck	Boost	Buck-Boost
k_f	$-DK_i$	$-(1+D)\frac{K_i}{2}$	$-DK_i$
k_r	$(1+D)\frac{K_i}{2}$	$D'\frac{K_i}{2}$	$D'\frac{K_i}{2}$
F_m	$\frac{D'}{S_n T_s}$		
F_c	$e^{sDT_s/4}$		

TABLE 3

Summary of Gain Parameters for Constant On-Time

	Buck	Boost	Buck-Boost
k_f	$-3D\frac{K_i}{2}$	$-(1+\frac{D}{2})K_i$	$-3D\frac{K_i}{2}$
k_r	$(1+\frac{D}{2})K_i$	$D'K_i$	$D'K_i$
F_m	$\frac{D}{S_f T_s}$		
F_c	$e^{sD'T_s/4}$		

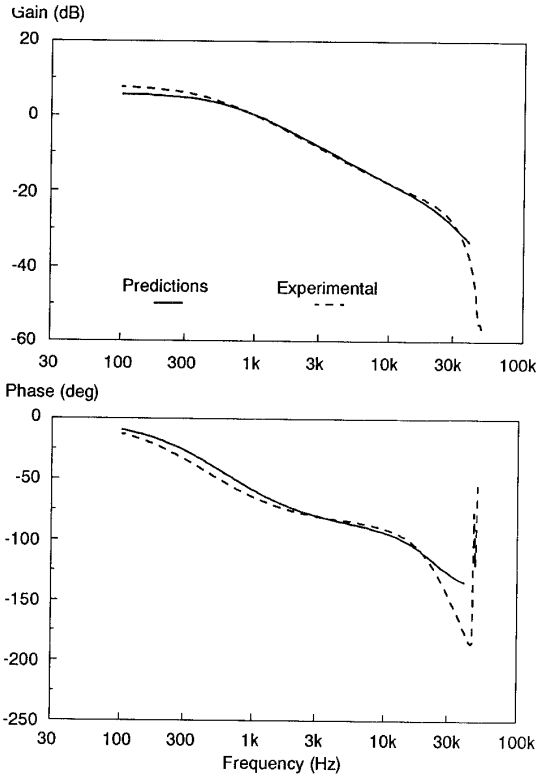

Fig. 8: Control-to-Output Measurement and Theory for Constant Off-Time, D = 0.1. *Measurement and theory agree very well for this transfer function up to 25 kHz, half the switching frequency.*

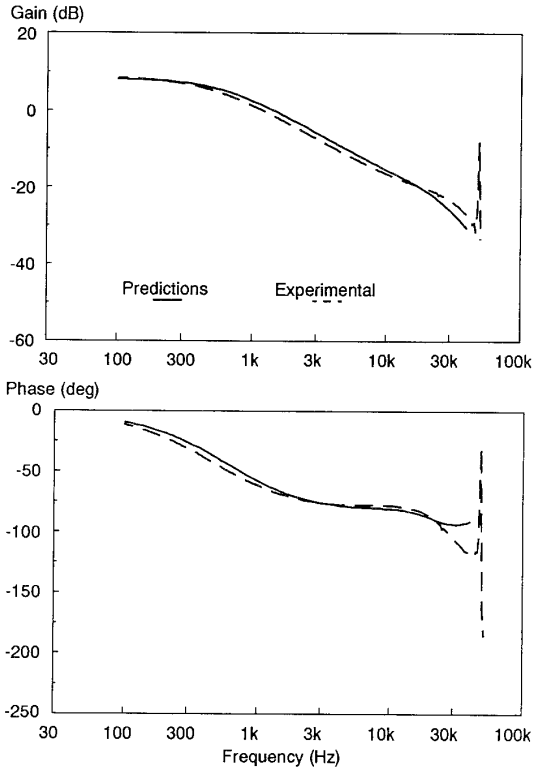

Fig. 9: Control-to-Output Measurement and Theory for Constant Off-Time, D = 0.4. *At higher duty cycles, the effect of the modulator phase lead F_c becomes significant. The double pole at half the switching frequency is still present in this transfer function.*

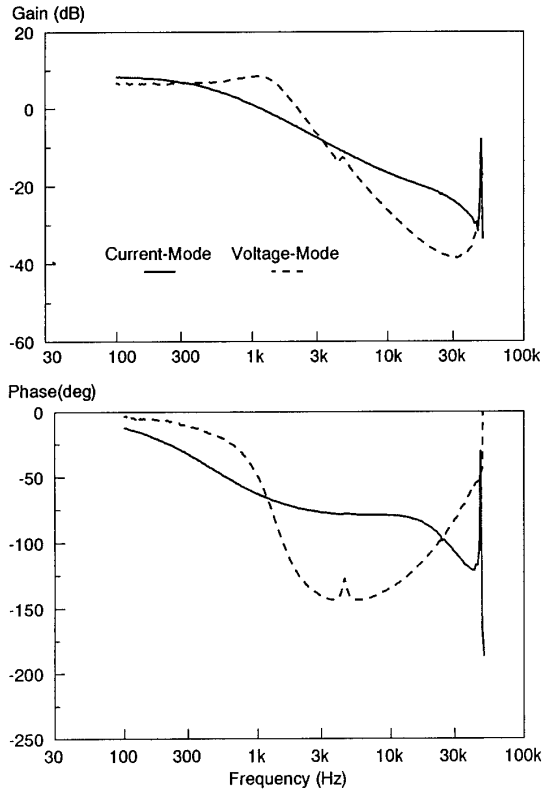

Fig. 10: Control-to-Output Measurement for Constant Off-Time, Voltage and Current-Mode Control. *The modulator phase characteristics also affect voltage mode control, obtained when the current sense resistor, R_i is zero. The intersection of the phase of the current-mode system and the voltage-mode system at half the switching frequency is further experimental confirmation of the existence of the double pole at half the switching frequency in the current mode transfer function. The benefits of current-mode control are apparent from this figure.*

Fig. 10 shows that the modulator phase lead also affects the voltage-mode control-to-output transfer function. The intersection of the phase of the current-mode and voltage-mode measurements at half the switching frequency offers further confirmation of the existence of the double pole at half the switching frequency with current-mode control.

IV. Discontinuous-Conduction Mode Models

When operating in the discontinuous mode, the PWM switch model for DCM, shown in Fig. 11, must be used. The power stage models are obtained by substituting this model in the circuits of Fig. 1b-d. Notice that the inductor current state is retained in this modeling technique.

The CCM converters needed sampled-data analysis to develop the small-signal models for current-mode control. This is not the case for converters operating in the DCM region. Fig. 12 shows the modulator waveforms for a converter operating with current-mode control in DCM. The control reference is used

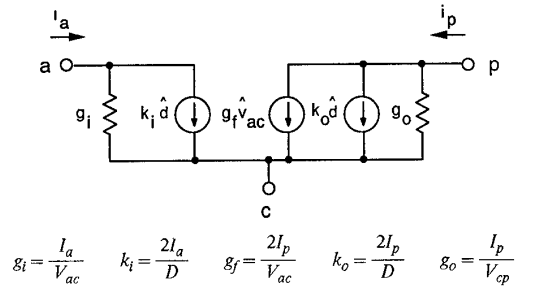

Fig. 11: PWM Switch Model for Discontinuous-Conduction Mode. *The PWM switch model for DCM is different from the model for CCM, but is also invariant for all PWM converters.*

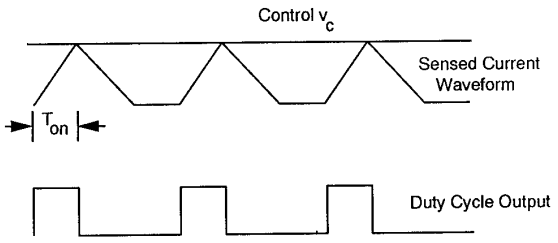

Fig. 12: Discontinuous-Conduction Modulator Waveforms for Current-Mode Control. *The sensed current waveform added to an external ramp is compared with a control signal, v_c, to provide the controlled duty cycle. Notice that the current ramp always starts from zero, and its slope is dependent upon the voltage across the inductor during the on-time. The modulator information could equally well be constructed by observing only the input and output voltages of the converter, and information about the inductor current is not needed.*

with the sensed inductor current to control the turn-off of the power switch. For DCM, the inductor current always starts at zero at turn-on. It is possible to achieve exactly the same effect as current-mode control by using a simple sawtooth ramp whose slope is determined by the input voltage, output voltage, and inductor value. Inductor current feedback is not necessary. The block diagram of Fig. 13 is, therefore, sufficient to completely model the current-mode feedback for DCM. The only task to be done to complete the model is to find the gains k_f and k_r.

The describing function of the modulator for converters in DCM with a controlled on-time is given by

$$T_{on} = \frac{v_c}{S_n + S_e} \tag{11}$$

The on-time slope, S_n, is a function of input voltage, output voltage, inductor value, and current-sense gain value, R_i. The small-signal perturbation due to changes in input and output voltage can therefore be found by taking the partial derivative of Eq. (11) with respect to each of these voltages. For example, for the buck converter with constant-frequency control, the small-signal gains are given by

$$\frac{\hat{d}}{\hat{v}_g} = \frac{-D}{D'V_g} \tag{12}$$

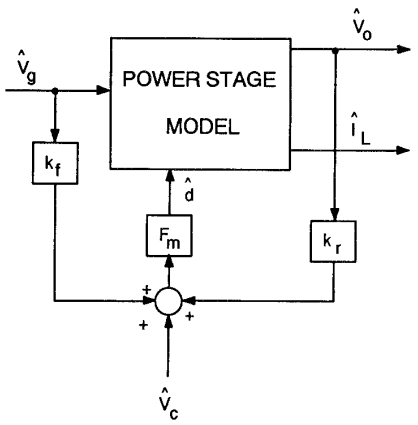

Fig. 13: Small-Signal Block Diagram for Current-Mode Control (DCM). *There is no feedback of inductor current in this block diagram, and no sampled-data modeling is needed. The feedforward blocks, k_f and k_r, provide the necessary control information.*

and

$$\frac{\hat{d}}{\hat{v}_o} = \frac{D}{D'V_g} \tag{13}$$

In the model of Fig. 13, perturbations in the duty cycle are given by the product of the gain blocks k_f and k_r, and the modulator gain, F_m. This representation provides a more convenient model. The necessary gains can be found by dividing Eqs. (12-13) by the modulator gain. The results of the analysis are presented in Table 4, for both constant-frequency and constant off-time control. Constant on-time current-mode control cannot be implemented since there is no current signal available at the end of the off-time in DCM.

The resulting models show several interesting effects obtained with current-mode control of DCM converters. The buck converter is especially interesting since it has a positive feedback term for k_r which can cause instability under the correct conditions. This effect has been noted in previously [10]. The control-to-output transfer function of the buck converter in DCM with constant frequency control is easily obtained from the block diagram of Fig. 13. This gain is given by

$$\frac{\frac{\hat{v}_o}{\hat{v}_c}}{} = \frac{F_m \frac{\hat{v}_o}{\hat{d}}}{1 - k_r F_m \frac{\hat{v}_o}{\hat{d}}} \tag{14}$$

The transfer function for the power stage can be found from the PWM switch model for DCM operation to give [7]

$$\frac{\hat{v}_o}{\hat{d}} = H_d \frac{1 + \frac{s}{\omega_{z1}}}{(1 + \frac{s}{\omega_{p1}})(1 + \frac{s}{\omega_{p2}})} \tag{15}$$

where

$$H_d = \frac{2V_o}{D} \frac{1 - M}{2 - M} \tag{16}$$

TABLE 4

Summary of Gain Parameters for DCM

	Buck	Boost	Buck-Boost
k_f	$-DK_i$	$-DK_i$	$-DK_i$
k_r	DK_i	0	0
F_m	$\frac{1}{(S_n + S_e)T_s}$ (Constant Frequency) $\frac{D'}{S_n T_s} e^{sDT_s/4}$ (Constant Off Time)		

$$\omega_{z1} = \frac{1}{CR_c} \tag{17}$$

$$\omega_{p1} = \frac{1}{CR} \frac{2 - M}{1 - M} \tag{18}$$

$$\omega_{p2} = 2F_s(\frac{M}{D})^2 \tag{19}$$

Substituting for each of the gains in Eq. (14), and realizing that $\omega_{p1} << \omega_{z1}$ and $\omega_{p1} << \omega_{p2}$, the control-to-output is derived to give:

$$\frac{\hat{v}_o}{\hat{v}_c} = F_m H_c \frac{1 + \frac{s}{\omega_{z1}}}{(1 + \frac{s}{\omega_{p1}'})(1 + \frac{s}{\omega_{p2}})} \tag{20}$$

where

$$H_c = \frac{2m_c V_o}{D} \frac{1 - M}{2m_c - (2 + mc)M} \tag{21}$$

$$\omega_{p1}' = \frac{1}{CR} \frac{2m_c - (2 + m_c)M}{m_c(1 - M)} \tag{22}$$

This transfer function shows the behavior of the constant-frequency buck converter with current-mode control in DCM. The instability mechanism is quite different from that observed with CCM. The low-frequency pole of Eq. (20), ω_{p1}' , is a function of the conversion ratio, M , of the converter. If no external ramp is used ($m_c = 1$), the pole moves to the origin at a conversion ratio of two-thirds, and into the right-half plane for higher conversion ratios. This effect can be mitigated by the addition of an external ramp to allow higher operating duty cycles. The use of the external ramp is recommended under all conditions for a buck converter with current mode control.

Fig. 14 shows predictions given by the transfer function of Eq. (20), and experimental measurements for the control-to-output transfer function with the current loop closed. From the gain curves for M = 0.22 and M = 0.64, the migration of the low frequency pole towards the zero-frequency axis as the conversion ratio increases can clearly be seen. The low-frequency phase plots also confirm this pole movement. The measurements and theoretical data agree well for low values of M at

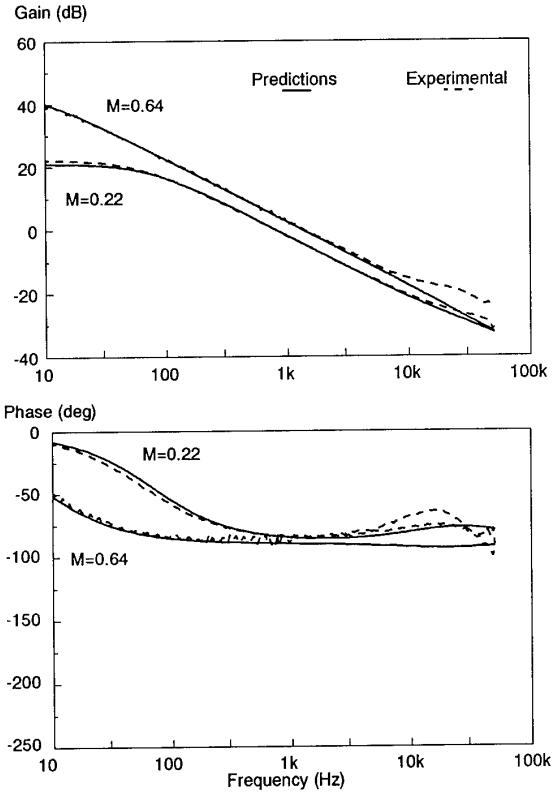

Fig. 14: Control-Output Transfer Function for Buck Converter (DCM). *As the conversion ratio of the converter increases, the dominant pole of the system moves towards the zero axis. When the conversion ratio exceeds 0.67, this pole crosses into the right-half plane, and the system becomes unstable.*

all frequencies. For higher values of M, the measurements deviated from theory at higher frequencies.

It should be pointed out that the buck converter was very difficult to hold stable under these conditions. In addition to the low-frequency pole which made the dc gain of the system very high, parasitic ringing of device capacitance when the inductor current went to zero seemed to affect the measurements, even when these parasitics were minimized and snubbed. These effects may have caused the deviations at higher duty cycles.

An additional interesting characteristic can be demonstrated for the constant-frequency flyback converter, using the model for current-mode DCM operation. The feedforward term k_f for this case provides complete nulling of input-voltage perturbations, giving an audio-susceptibility of zero.

V. Conclusions

A new current-mode control model has been extended for the analysis of converters with constant on-time control and constant off-time control. The model for these control schemes is simple to use, but has an additional modulator phase-lead term which did not occur for the constant-frequency modulator. Current-loop instability, which occurs with constant-frequency control, is eliminated with constant on- and off-time control. Even though the characteristics of the current loop are the same for the different control schemes, the reduced modulator gain of the variable frequency control prevents the instability. Like the constant-frequency model, the control-to-output transfer function has a double pole at half the switching frequency, but with a fixed Q of $2/\pi$. Experimental results have confirmed the validity of the model up to half the switching frequency.

The DCM current-mode model was developed, and shown to have a simple form without a current feedback loop appearing in the model. Feedforward gain terms from the input and output voltages are sufficient to predict all of the phenomena observed with DCM current-mode control. The inherent instability of the buck converter operating in DCM with current-mode control was confirmed analytically and experimentally for high conversion ratios.

References

1. R.B. Ridley, "A New Small-Signal Model for Current-Mode Control" Power Conversion and Intelligent Motion Conference proceedings, October 16-19, 1989.

2. R.D. Middlebrook, "Topics in Multiple-Loop Regulators and Current-Mode Programming," IEEE Power Electronics Specialists Conference proceedings, June 24-28, 1985.

3. G.C. Verghese, C.A. Bruzos, K.N. Mahabir, "Averaged and Sampled-Data Models for Current Mode Control: A Reexamination," IEEE Power Electronics Specialists Conference proceedings, June 26-29, 1989.

4. L.H. Dixon, "Closing the Feedback Loop," Appendix C, Unitrode Power Supply Design Seminar, pp. 2C1-2C18, 1983.

5. F.C. Lee, M.F. Mahmoud, Y. Yu, "Design Handbook for a Standardized Control Module for DC-to-DC Converters," Volume I, NASA CR-165172, April, 1980. See also F.C. Lee, Y. Yu, M.F. Mahmoud, "A Unified Analysis and Design Procedure for a Standardized Control Module for DC-DC Switching Regulators," Power Electronics Specialists Conference proceedings, pp.284-301, June 16-20, 1980.

6. A.R. Brown, R.D. Middlebrook, "Sampled-Data Modeling of Switching Regulators," Power Electronics Specialists Conference proceedings, pp. 349-369, June 29-July 3, 1981.

7. V. Vorperian, "Simplified Analysis of PWM Converters Using the Model of the PWM Switch: Parts I and II," IEEE Transactions on Aerospace and Electronic Systems, March 1990, Vol. 26, No. 2. See also VPEC Newsletter "Current," Fall 1988, and Spring 1989 Issues, Virginia Polytechnic Institute and State University.

8. B.H. Cho, F.C. Lee, "Measurement of Loop Gain with the Digital Modulator," IEEE Power Electronics Specialists Conference, June 18-21, 1984.

9. R.D. Middlebrook, "Predicting Modulator Phase Lag in PWM Converter Feedback Loops," Powercon 8, April 27-30, 1981.

10. R.P.E. Tymerski, K.C. Daly, "Modelling and Analysis of Current-Programmed DC/DC Converters," Journal of Electrical and Electronics Engineering, Australia, Vol 5, No. 1, March 1985.